

# Dissipation and velocity distribution at the shear-driven jamming transition

Peter Olsson

Department of Physics, Umeå University, 901 87 Umeå, Sweden

(Dated: March 16, 2019)

We investigate energy dissipation and the distribution of particle velocities at the jamming transition for overdamped shear-driven frictionless disks in two dimensions at zero temperature. We find that the dissipation is caused by the fastest particles and that the fraction of particles responsible for the dissipation decreases towards zero as jamming is approached. This is related to the distribution of particle velocities that develops an algebraic tail  $\sim v^{-3}$ . This wide distribution also implies that concepts like “typical velocity” may no longer be used, which has implications for analytical approaches to jamming.

PACS numbers: 64.60.-i, 64.70.Q-, 45.70.-n

The hypothesis that the slowing down of the dynamics in systems as different as supercooled liquids, granular materials, colloids, foams, and emulsions, have a common origin in the properties of a critical point, point J[1], has inspired a great amount of work on jamming the last decade. Several models have been used to try and pinpoint the properties of this jamming transition. Some of them have centered around a greatly simplified numerical model of spheres with contact-only interaction. One important branch has been to examine the properties of randomly generated static packings[2] whereas another has been to study the jamming transition through simulations of elastic particles under steady shear[3].

A key feature of jamming is the approach of the contact number  $z$  to the isostatic number  $z_{\text{iso}}$  which is just enough for mechanical stability. It has recently been shown[4] that this is directly linked to the divergence of  $\eta_p \equiv p/\dot{\gamma}$ —the pressure equivalent of the shear viscosity. A related phenomenon is the increase in particle velocity as  $\phi \rightarrow \phi_J$ [5, 6]. This is related to the distribution of particle displacements due to a small shear increment which has been determined both in experiments of sheared granular materials[7] and in quasistatic simulations[5, 7]. It was there found that this distribution is sufficiently wide that the non-Gaussian parameter  $\langle \Delta y^4 \rangle / 3 \langle (\Delta y)^2 \rangle - 1$  diverges as  $\phi_J$  is approached from below, granted that the shear step is sufficiently small.

In this Letter we show that there is more to the particle velocity distribution than has so far been realized. Dissipation is mainly caused by the fastest particles and we find that the fraction of particles that are responsible for the dissipation decreases towards zero as jamming is approached. This behavior is related to an algebraic tail,  $P(v) \sim v^{-3}$ , in the velocity distribution and we show that the velocity histograms determined at the jamming density approach this limiting behavior as  $\dot{\gamma} \rightarrow 0$ . Since rheology and dissipation are linked through power balance, the understanding of this phenomenon is right at the center of the phenomenon of shear-driven jamming. We also note that this finding has profound consequence for analytical approaches to jamming since it implies that differ-

ent measures of the velocity behave differently and that concepts like “typical velocity” therefore become useless.

Following O’Hern *et al.*[2] we use a simple model of bi-disperse frictionless soft disks in two dimensions with equal numbers of disks with two different radii in the ratio 1.4. Length is measured in units of the diameter of the small particles,  $d_s$ . We use Lees-Edwards boundary conditions[8] to introduce a time-dependent shear strain  $\gamma = t\dot{\gamma}$ . With periodic boundary conditions on the coordinates  $x_i$  and  $y_i$  in an  $L \times L$  system, the position of particle  $i$  in a box with strain  $\gamma$  is defined as  $\mathbf{r}_i = (x_i + \gamma y_i, y_i)$ . The ordinary velocity is  $\mathbf{v}_i^{\text{tot}} = \dot{\mathbf{r}}_i$ , but in the following we will consider the non-affine velocity,  $\mathbf{v}_i = \mathbf{v}_i^{\text{tot}} - \mathbf{v}_R(\mathbf{r}_i)$  where  $\mathbf{v}_R(\mathbf{r}_i) \equiv \dot{\gamma} y_i \hat{x}$  is a uniform shear velocity. With  $r_{ij}$  the distance between the centers of two particles and  $d_{ij}$  the sum of their radii, the relative overlap is  $\delta_{ij} = 1 - r_{ij}/d_{ij}$  and the interaction between overlapping particles is  $V(r_{ij}) = \epsilon \delta_{ij}^2/2$ ; we take  $\epsilon = 1$ . The force on particle  $i$  from particle  $j$  is  $\mathbf{f}_{ij}^{\text{el}} = -\nabla_i V(r_{ij})$ . The simulations are performed at zero temperature.

We consider two different models for the energy dissipation. In both cases the interaction force is  $\mathbf{f}_i^{\text{el}} = \sum_j \mathbf{f}_{ij}^{\text{el}}$  where the sum extends over all particles  $j$  in contact with  $i$ , and the equation of motion is

$$\mathbf{f}_i^{\text{el}} + \mathbf{f}_i^{\text{dis}} = m_i \ddot{\mathbf{r}}_i. \quad (1)$$

Most of our simulations have been done with the RD<sub>0</sub> (reservoir dissipation) model with the dissipating force

$$\mathbf{f}_{\text{RD},i}^{\text{dis}} = -k_d \mathbf{v}_i. \quad (2)$$

We take  $k_d = 1$ ,  $m_i = 0$ , and the time unit  $\tau_0 = d_s k_d / \epsilon$ . We simulate  $N = 65536$  particles with shear rates down to  $\dot{\gamma} = 10^{-10}$  and integrate the equations of motion with the Heuns method with time step  $\Delta t = 0.2\tau_0$ .

Some additional simulations have also been done with the CD<sub>0</sub> model (CD for “contact dissipation”) with dissipation due to velocity differences of disks in contact[3, 9]. Details of the simulations may be found elsewhere[10].

A key quantity in the present letter is the energy dissipation. We here just remark that this is a central quan-

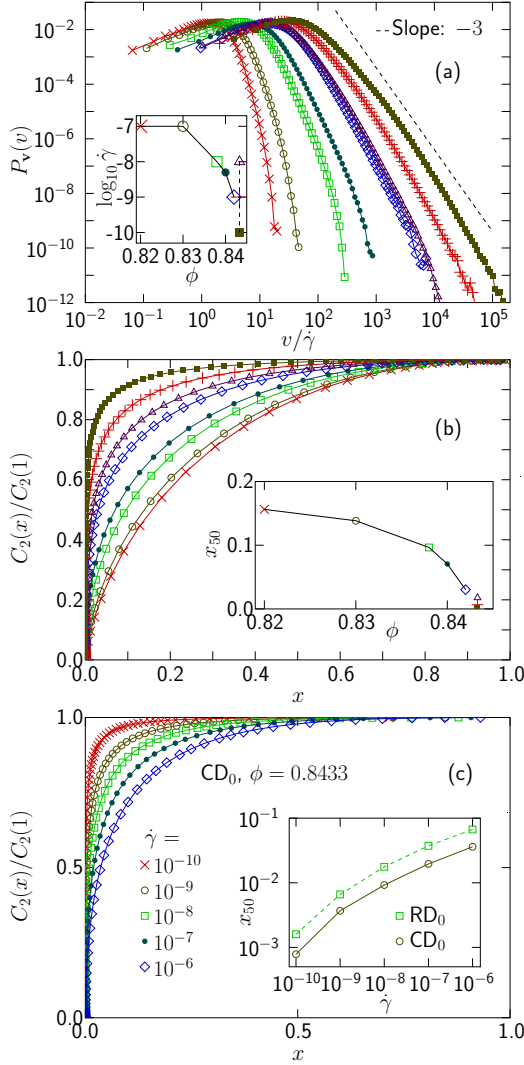


FIG. 1. (Color online) Velocity distribution and dissipation. Panel (a) shows the velocity distribution function  $P_v(v)$  vs  $v/\gamma$  with simulation parameters  $(\phi, \dot{\gamma})$  and symbols as shown by the inset. The dashed line has slope  $-3$ . Panel (b) shows the part of the dissipated power which is dissipated by the fraction  $x$  of the fastest particles. Panel (c) shows the same quantity for the CD<sub>0</sub> model. These data are at  $\phi = 0.8433 \approx \phi_J$  and five different shear rates. The insets of panels (b) and (c) are  $x_{50}$ —the fraction of particles needed to dissipate 50% of the power. The inset of panel (b) shows that  $x_{50}$  for the RD<sub>0</sub> model decreases as  $\phi$  increases whereas the inset of panel (c) shows  $x_{50}$  at  $\phi_J$  decreasing with  $\dot{\gamma}$  for both RD<sub>0</sub> and CD<sub>0</sub>.

ity due to the relation between dissipation and rheology from power balance,  $V\sigma\dot{\gamma} = k_d \langle \sum_i \mathbf{v}_i^2 \rangle$  [11], and we therefore believe that the considerations here may be instrumental in developing a better understanding of shear-driven jamming.

We will now show that most of the energy is dissipated by a small fraction of fast particles and, furthermore, that the fraction of particles needed to dissipate a given part of the power decreases as jamming is approached.

Note that “fast” is here used in a relative sense. For low  $\dot{\gamma}$  all particles are slow, it is only  $v/\gamma$  that can be big. To study the dissipation we introduce the velocity distribution function  $P_v(v)$  such that  $P_v(v)dv$  is the fraction of particles with velocity  $v \leq |\mathbf{v}| < v + dv$ . Fig. 1(a) shows  $P_v(v)$  vs  $v/\gamma$  both at five densities below  $\phi_J$ , and for three different shear rates at  $\phi_J$ . (To get histograms of good quality down to small  $P_v$  we use bins that are equally spaced in  $\ln v$ .) The different simulation parameters  $(\phi, \dot{\gamma})$  and their corresponding symbols are shown in the inset of panel (a). The points connected by solid lines and dash lines, respectively, show two different ways to approach jamming. The solid line connects  $(\phi, \dot{\gamma})$  at  $\phi < \phi_J$  and at sufficiently low  $\dot{\gamma}$  to be very close to the hard disk limit. The dashed line connects three points at  $\phi = 0.8433 \approx \phi_J$ . Here jamming is approached as  $\dot{\gamma} \rightarrow 0$ .

To study the dissipation with focus on the fast particles we define

$$x(v) = \int_v^\infty P_v(v') dv', \quad \bar{C}_2(v) = \int_v^\infty P_v(v') v'^2 dv'. \quad (3)$$

Here  $x(v)$  is the fraction of fast particles with  $|\mathbf{v}| > v$  and  $k_d \bar{C}_2(v)$  is the dissipating power due to the same particles. We also define  $C_2(x) = \bar{C}_2(v(x))$ , where  $v(x)$  is the inverse of  $x(v)$ . Fig. 1(b) shows the normalized  $C_2$  vs  $x$  for the data in panel (a). The faster particles always dominate the dissipation but this effect becomes more pronounced—the curves get steeper—as jamming is approached; a smaller fraction of particles is then needed for a given part of the dissipation. As a simple quantitative measure we introduce  $x_{50}$ , shown in the inset of panel (b), as the fraction of the fastest particles that dissipates 50% of the power. For the hard disk limit (solid line)  $x_{50}$  decreases as  $\phi$  increases towards  $\phi_J$ . The behavior of  $x_{50}$  at  $\phi = 0.8433 \approx \phi_J$  is shown by the open squares in the inset of panel (c);  $x_{50}$  decreases with decreasing  $\dot{\gamma}$  and gets as low as 0.16% at the lowest shear rate,  $\dot{\gamma} = 10^{-10}$ . We believe that this localization of the dissipation to a few faster particles is related to plastic events or avalanches that are found above  $\phi_J$ , as already speculated by others [5].

Panel (c) shows that the CD<sub>0</sub> model behaves similarly. In this model it is the velocity differences of contacting particles that is the quantity of interest rather than the non-affine velocity, and  $C_2$  is defined analogously. The main data in panel (c) is  $C_2(x)$  at  $\phi_J$  for the CD<sub>0</sub> model which is very similar to the three data sets at  $\phi_J$  in panel (a). As a more detailed comparison the inset of panel (c) shows  $x_{50}$  against  $\dot{\gamma}$  at  $\phi_J$  for both the RD<sub>0</sub> model and the CD<sub>0</sub> model, and it is clear that this fraction decreases with decreasing  $\dot{\gamma}$  in both models. The effect studied here is thus not just peculiar to the simpler RD<sub>0</sub> model.

The evidence from Fig. 1 strongly suggests that  $C_2(x)/C_2(1)$  approaches a step function as  $\phi \rightarrow \phi_J$  and  $\dot{\gamma} \rightarrow 0$ , and this is the main result from the first part of this Letter. In the remainder we will argue that this

finding has very specific implications for the velocity distribution and that it also implies that different measures of the typical velocity diverge differently.

For  $C_2(x)/C_2(1)$  to approach a step function the limiting distribution has to have a tail

$$P_{\mathbf{v}}(v) \sim v^{-3}, \quad (4)$$

since that makes  $C_2(v)$  diverge. Before turning to more elaborate analyses we note that Fig. 1(a) gives some support for the slope = -3 (given by the dashed line) for the limiting behavior of the velocity distribution at  $\phi_J$  as  $\dot{\gamma} \rightarrow 0$ .

For the further analysis it is important to understand the origin of the wide distribution. We note that the non-affine velocity in the RD<sub>0</sub> model is related to the sum of all (repulsive) contact forces that act on the particle. The non-affine velocity of particle  $i$  is  $\mathbf{v}_i = \sum_j \mathbf{f}_{ij}^{\text{el}}/k_d$ . Close to jamming, the forces on most particles almost cancel one another out, and the total force is typically very small compared to the average force,  $f_i^{\text{el}} \ll f_{ij}^{\text{el}}$ , as has also been noted by others[12]. There are however some particles for which the forces don't balance one another out, and the velocity of these particles can then be much larger than the average velocity. The wide distribution is thus due to the big difference between the individual forces and the typical total force.

A consequence of this picture is that the maximum velocity is bounded by the typical  $f_{ij}^{\text{el}}$  which means that the possibly algebraic distribution is cut off by an exponential factor  $e^{-v/v_c}$ , where  $v_c \sim f_{ij}/k_d \sim p/(k_d d_s)$ . (This also suggests  $v_c/\dot{\gamma} \sim \eta_p$ .) This behavior is seen in Fig. 1(a) as the approximately rectilinear (i.e. algebraic) behaviors for intermediate values of  $P_{\mathbf{v}}(v)$  turn into more rapid decays at higher velocities. One therefore expects the tails in the distributions to be described by

$$P(v) \sim v^{-r} e^{-v/v_c}. \quad (5)$$

The exponentially decaying factor has to be included, and becomes a complicating factor, when one attempts to determine  $r$  from  $P(v)$ . Since the cutoff velocity moves farther out in the tail as  $\dot{\gamma}$  decreases it will however not affect the divergence of  $C_2$  that we expect at  $\phi_J$  as  $\dot{\gamma} \rightarrow 0$ .

For the determination of  $r$  we have found it convenient to use the distribution of the absolute value of the  $y$  component of the velocity. This quantity differs from  $P_{\mathbf{v}}$  in that it approaches a constant at small velocities, and this makes it easier to find an analytical expression that fits the data. We introduce the notation  $\tilde{v}_y = v_y/\dot{\gamma}$  and  $P(\tilde{v}_y)$  for the distribution. Fig. 2(a) shows  $P(\tilde{v}_y)$  for several different  $\dot{\gamma}$  at  $\phi = 0.8433 \approx \phi_J$ .

To determine both the exponent  $r$  and the cutoff velocity  $\tilde{v}_c$  we fit  $P(\tilde{v}_y)$  to

$$P(\tilde{v}_y) = \frac{A e^{-\tilde{v}_y/\tilde{v}_c}}{1 + A_1 \tilde{v}_y^a + A_2 \tilde{v}_y^r}, \quad (6)$$

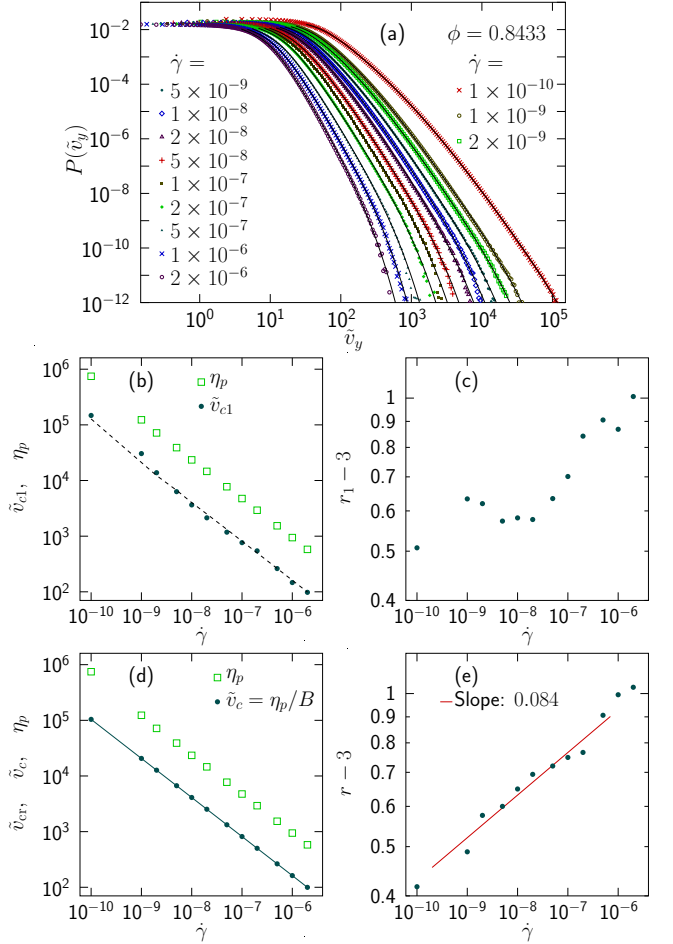


FIG. 2. (Color online) Velocity distribution and the determination of the exponent  $r$  for different  $\dot{\gamma}$  at  $\phi = 0.8433 \approx \phi_J$ . Panel (a) is the velocity distribution  $P(\tilde{v}_y)$ . Panels (b) and (c) show  $\tilde{v}_{c1}$  and  $r_1 - 3$  vs  $\dot{\gamma}$  from direct fits to Eq. (6). The bad precision in  $r_1$  is to some extent due to the covariation of  $r_1$  and  $\tilde{v}_{c1}$ . From the expectation that  $\tilde{v}_c \propto \eta_p$ , with the proportionality constant  $1/B$  from panel (b), we fix  $\tilde{v}_c = \eta_p/B$ , see panel (d), and do another fit that gives values for  $r$  that fluctuate considerably less and allow for the determination of the exponent. Fitting  $r - 3 \sim \dot{\gamma}^{q_r}$  for  $10^{-9} \leq \dot{\gamma} \leq 5 \times 10^{-7}$  gives  $q_r = 0.084 \pm 0.02$ .

which is an expression that crosses over from a constant at small  $\tilde{v}_y$  to a large- $\tilde{v}_y$  tail with  $\tilde{v}_y^{-r} e^{-\tilde{v}_y/\tilde{v}_c}$ . This crossover is somewhat different for the different data sets and we chose to handle that through an additional term in the denominator,  $A_1 \tilde{v}_y^a$ , with  $a < r$  (typically  $a \approx 2$ ). Panel (b) of Fig. 2 shows  $\tilde{v}_{c1}$  obtained in this fit by solid dots together with  $\eta_p = p/\dot{\gamma}$  given by open squares. ( $\tilde{v}_{c1}$  and  $r_1$  are the fitting parameters from the first fit to Eq. (6).) This figure suggests that these two quantities behave the same, and we determine  $B = \langle \eta_p/\tilde{v}_{c1} \rangle \approx 5.8$ ; the dashed line shows  $\eta_p/B$ .

To test the hypothesis that the limiting velocity distribution at jamming is  $\tilde{v}_y^{-3}$ , i.e. that  $r \rightarrow 3$ , Fig. 2(c) shows  $r_1 - 3$  against  $\dot{\gamma}$ . This figure does provide some

evidence that  $r_1$  decreases with decreasing  $\dot{\gamma}$ , but the data are much too noisy to allow for any characterization of this decay. A reason for the bad precision in this determination is the covariation of  $r_1$  and  $\tilde{v}_{c1}$ , which is there since a somewhat too large  $r_1$ —which would give a faster decay—may be compensated for by a somewhat too large  $\tilde{v}_{c1}$ —which would lead to a slower decay. To try and reduce these fluctuations we assume that  $\tilde{v}_c \propto \eta_p$  (as both argued above and suggested by the data in panel (b)) and make another fit to Eq. (6) keeping  $\tilde{v}_c = \eta_p/B$  fixed. This approach gives  $r$  with considerably smaller fluctuations, as shown in panel (e). An algebraic fit gives  $r - 3 \sim \dot{\gamma}^{q_r}$  with  $q_r = 0.084 \pm 0.02$ .

A significant implication of the wide velocity distribution is that different measures of the typical velocity will behave differently. For the discussion we define

$$\tilde{v}_1 = \langle |\tilde{v}_y| \rangle, \quad \text{and} \quad \tilde{v}_{\text{rms}}^2 = \langle \tilde{v}_y^2 \rangle. \quad (7)$$

With a simplified distribution that allows for analytical calculations,

$$P(\tilde{v}_y) = \begin{cases} C, & \tilde{v}_y < \tilde{v}_s, \\ C(\tilde{v}_y/\tilde{v}_s)^{-r}, & \tilde{v}_y \geq \tilde{v}_s, \end{cases} \quad (8)$$

the different characteristic velocities become

$$\tilde{v}_1 = \frac{\frac{1}{2} + (r-2)^{-1}}{1 + (r-1)^{-1}} \tilde{v}_s, \quad \tilde{v}_{\text{rms}}^2 = \frac{\frac{1}{3} + (r-3)^{-1}}{1 + (r-1)^{-1}} \tilde{v}_s^2. \quad (9)$$

What we have in mind here is a situation where  $\tilde{v}_1$  diverges due to the behavior of  $\tilde{v}_s$  whereas there is an additional diverging contribution to  $\tilde{v}_{\text{rms}}$  due to the behavior of  $r$ . When  $r$  approaches 3, i.e. for  $(r-3)^{-1} \gg 1$ , these equations give

$$\tilde{v}_{\text{rms}}^2/\tilde{v}_1^2 \sim \frac{1}{r-3}. \quad (10)$$

At  $\phi_J$  we may then make use of  $r - 3 \sim \dot{\gamma}^{q_r}$  to get

$$\tilde{v}_{\text{rms}}^2/\tilde{v}_1^2 \sim \dot{\gamma}^{-q_r}, \quad \phi = \phi_J, \quad (11)$$

which shows that the two different measures of the velocity diverge differently.

The simulations also show very clearly that  $\tilde{v}_{\text{rms}}$  and  $\tilde{v}_1$  diverge differently. Fig. 3(a) shows  $\tilde{v}_{\text{rms}}$  and  $\tilde{v}_1$  at  $\phi_J$  vs  $\dot{\gamma}$ . Both quantities seem to diverge algebraically,  $\tilde{v}_{\text{rms}} \sim \dot{\gamma}^{-\beta/2z\nu} \sim \dot{\gamma}^{-0.34}$  and  $\tilde{v}_1 \sim \dot{\gamma}^{-u_v/z\nu} \sim \dot{\gamma}^{-0.29}$ . [The scaling expressions follow by taking  $b = \dot{\gamma}^{-1/z}$  in  $\mathcal{O}(\phi, \dot{\gamma}) = b^{u_O/\nu} g_O((\phi_J - \phi)b^{1/\nu}, \dot{\gamma}b^z)$ [13] with the scaling dimension  $u_O$  equal to  $u_v$  for  $\tilde{v}_1$  and  $\beta/2$  for  $\tilde{v}_{\text{rms}}$ . The latter follows from  $\eta \sim \tilde{v}_{\text{rms}}^2$  and  $\eta(\phi, \dot{\gamma} \rightarrow 0) \sim (\phi_J - \phi)^{-\beta}$ .] For the quantity in Eq. (11) this becomes

$$\tilde{v}_{\text{rms}}^2/\tilde{v}_1^2 \sim \dot{\gamma}^{-(\beta-2u_v)/z\nu}, \quad (12)$$

and the numerics gives  $(\beta - 2u_v)/z\nu = 0.10$ . This is in good agreement with  $q_r = 0.084 \pm 0.02$  from Fig. 2(e), that should correspond to the low- $\dot{\gamma}$  limit.

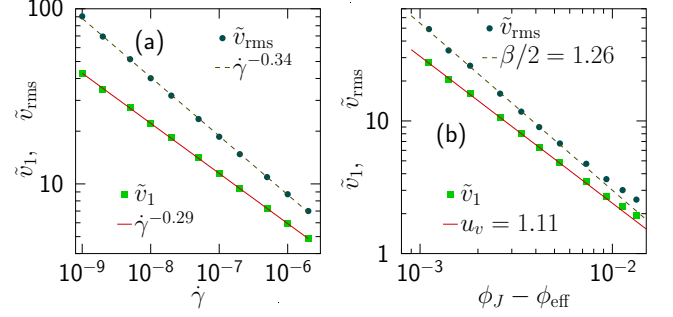


FIG. 3. (Color online) Two different measures of the “typical velocity”. Panel (a) shows  $\tilde{v}_{\text{rms}}$  and  $\tilde{v}_1$  for  $\phi = 0.8433 \approx \phi_J$  vs  $\dot{\gamma}$ . Panel (b) shows the same quantities for data below  $\phi_J$  plotted vs distance to jamming; only the points with  $\phi_J - \phi_{\text{eff}} < 0.006$  were used for the fits. The lines are  $\sim (\phi_J - \phi_{\text{eff}})^{-u_v}$  and  $\sim (\phi_J - \phi_{\text{eff}})^{-\beta/2}$  where  $\phi_{\text{eff}}$  is the effective density.

Though most of our analyses in this Letter have been performed at  $\phi_J$ , it is instructive to examine the same quantities with data below  $\phi_J$ , close to the hard disk limit. Fig. 3(b) shows how  $\tilde{v}_{\text{rms}}$  and  $\tilde{v}_1$  diverge as the jamming density is approached from below. For hard disks the expected behaviors are especially simple,

$$\tilde{v}_1^{\text{hd}}(\phi) \sim (\phi_J - \phi)^{-u_v}, \quad \tilde{v}_{\text{rms}}^{\text{hd}}(\phi) \sim (\phi_J - \phi)^{-\beta/2}, \quad (13)$$

and for best possible precision in the analysis of our soft disk data, we make use of the effective-density mapping of soft disks onto hard disks,  $\mathcal{O}^{\text{hd}}(\phi_{\text{eff}}) = \mathcal{O}(\phi, \dot{\gamma})$ , where the effective density is  $\phi_{\text{eff}} = \phi - cE^{1/2y}$ , with  $c = 1.53$  and  $y = 1.09$ , as detailed in Ref. [14]. Fig. 3(b) shows  $\tilde{v}_{\text{rms}}$  and  $\tilde{v}_1$  against  $\phi_J - \phi_{\text{eff}}$ . The solid line gives the exponent  $u_v = 1.11$  in very good agreement with  $\ell_{\Delta} \sim (\phi_J - \phi)^{-1.1}$  for the particle “velocity” in Ref. [5]. The dashed line gives  $\beta/2 = 1.26$ . This value,  $\beta = 2.52$ , is somewhat low in comparison to recent estimates[13], but this is also consistent with earlier findings that neglect of corrections to scaling in the analysis of  $\eta$  tend to underestimate the exponent[13]. Note that the exponents from Fig. 3(a) and (b) are consistent when using  $1/z\nu = 0.26$ [13].

To summarize, we have found that the fraction of particles that are responsible for the energy dissipation decreases towards zero as jamming is approached. This suggests a tail,  $P(v) \sim v^{-3}$ , in the velocity distribution function at jamming, which is also confirmed by direct analyses. The presence of this tail implies that different measures of the velocity behave differently close to jamming. Concepts like “typical” velocity are then no longer useful and this should have profound consequences for all kinds of analytical approaches to shear-driven jamming.

I thank S. Teitel for many discussions and a critical reading of the manuscript. This work was supported by the Swedish Research Council Grant No. 2010-3725. Simulations were performed on resources provided by the Swedish National Infrastructure for Computing (SNIC)

at PDC and HPC2N.

---

[1] A. J. Liu and S. R. Nagel, *Nature (London)* **396**, 21 (1998)

[2] C. S. O'Hern, L. E. Silbert, A. J. Liu, and S. R. Nagel, *Phys. Rev. E* **68**, 011306 (2003)

[3] D. J. Durian, *Phys. Rev. Lett.* **75**, 4780 (1995)

[4] E. Lerner, G. Düring, and M. Wyart, *PNAS* **109**, 4798 (2012)

[5] C. Heussinger, L. Berthier, and J.-L. Barrat, *Europhys. Lett.* **90**, 20005 (2010)

[6] B. Andreotti, J.-L. Barrat, and C. Heussinger, *Phys. Rev. Lett.* **109**, 105901 (2012)

[7] G. Marty and O. Dauchot, *Phys. Rev. Lett.* **94**, 015701 (2005)

[8] D. J. Evans and G. P. Morriss, *Statistical Mechanics of Nonequilibrium Liquids* (Academic Press, London, 1990)

[9] B. P. Tighe, E. Woldhuis, J. J. C. Remmers, W. van Saarloos, and M. van Hecke, *Phys. Rev. Lett.* **105**, 088303 (2010)

[10] D. Vågberg, P. Olsson, and S. Teitel, *Phys. Rev. Lett.* **113**, 148002 (2014)

[11] I. K. Ono, S. Tewari, S. A. Langer, and A. J. Liu, *Phys. Rev. E* **67**, 061503 (2003)

[12] E. DeGiuli, G. Düring, E. Lerner, and M. Wyart, *Phys. Rev. E* **91**, 062206 (2015)

[13] P. Olsson and S. Teitel, *Phys. Rev. E* **83**, 030302(R) (2011)

[14] P. Olsson and S. Teitel, *Phys. Rev. Lett.* **109**, 108001 (2012)